Host Species Restriction of Middle East Respiratory Syndrome Coronavirus through Its Receptor, Dipeptidyl Peptidase 4

Neeltje van Doremalen,[a] Kerri L. Miazgowicz,[a] Shauna Milne-Price,[a] Trenton Bushmaker,[a] Shelly Robertson,[a] Dana Scott,[b] Joerg Kinne,[c] Jason S. McLellan,[d] Jiang Zhu,[e] Vincent J. Munster[a]

Laboratory of Virology, Division of Intramural Research, National Institute of Allergy and Infectious Diseases, National Institutes of Health, Hamilton, Montana, USA[a]; Rocky Mountain Veterinary Branch, Division of Intramural Research, National Institute of Allergy and Infectious Diseases, National Institutes of Health, Hamilton, Montana, USA[b]; Central Veterinary Research Laboratories, Dubai, Dubai, United Arab Emirates[c]; Department of Biochemistry, Geisel School of Medicine at Dartmouth, Hanover, New Hampshire, USA[d]; Department of Immunology and Microbial Science and Department of Integrative Structural and Computational Biology, The Scripps Research Institute, La Jolla, California, USA[e]

ABSTRACT

Middle East respiratory syndrome coronavirus (MERS-CoV) emerged in 2012. Recently, the MERS-CoV receptor dipeptidyl peptidase 4 (DPP4) was identified and the specific interaction of the receptor-binding domain (RBD) of MERS-CoV spike protein and DPP4 was determined by crystallography. Animal studies identified rhesus macaques but not hamsters, ferrets, or mice to be susceptible for MERS-CoV. Here, we investigated the role of DPP4 in this observed species tropism. Cell lines of human and nonhuman primate origin were permissive of MERS-CoV, whereas hamster, ferret, or mouse cell lines were not, despite the presence of DPP4. Expression of human DPP4 in nonsusceptible BHK and ferret cells enabled MERS-CoV replication, whereas expression of hamster or ferret DPP4 did not. Modeling the binding energies of MERS-CoV spike protein RBD to DPP4 of human (susceptible) or hamster (nonsusceptible) identified five amino acid residues involved in the DPP4-RBD interaction. Expression of hamster DPP4 containing the five human DPP4 amino acids rendered BHK cells susceptible to MERS-CoV, whereas expression of human DPP4 containing the five hamster DPP4 amino acids did not. Using the same approach, the potential of MERS-CoV to utilize the DPP4s of common Middle Eastern livestock was investigated. Modeling of the DPP4 and MERS-CoV RBD interaction predicted the ability of MERS-CoV to bind the DPP4s of camel, goat, cow, and sheep. Expression of the DPP4s of these species on BHK cells supported MERS-CoV replication. This suggests, together with the abundant DPP4 presence in the respiratory tract, that these species might be able to function as a MERS-CoV intermediate reservoir.

IMPORTANCE

The ongoing outbreak of Middle East respiratory syndrome coronavirus (MERS-CoV) has caused 701 laboratory-confirmed cases to date, with 249 fatalities. Although bats and dromedary camels have been identified as potential MERS-CoV hosts, the virus has so far not been isolated from any species other than humans. The inability of MERS-CoV to infect commonly used animal models, such as hamster, mice, and ferrets, indicates the presence of a species barrier. We show that the MERS-CoV receptor DPP4 plays a pivotal role in the observed species tropism of MERS-CoV and subsequently identified the amino acids in DPP4 responsible for this restriction. Using a combined modeling and experimental approach, we predict that, based on the ability of MERS-CoV to utilize the DPP4 of common Middle East livestock species, such as camels, goats, sheep, and cows, these form a potential MERS-CoV intermediate host reservoir species.

The Middle East respiratory syndrome coronavirus (MERS-CoV) was first identified in 2012 in a patient from Saudi-Arabia (1). To date, 701 laboratory-confirmed cases have been reported in eight different countries, with an estimated 35% case fatality rate (2). MERS-CoV is a positive-strand RNA virus belonging to the C lineage within the *Betacoronavirus* genus and is genetically closely related to coronavirus sequences obtained from insectivorous bats originating from Europe, Asia, Africa, and the Middle East (1, 3–5). The detection of MERS-CoV neutralizing antibodies and the recovery of viral sequences and virus in dromedary camels across the countries of the Middle East suggest the potential involvement of an intermediate reservoir in the emergence of MERS-CoV in humans (6–10). Phylogenetic analysis of MERS-CoV genomes obtained from 43 human cases in Saudi Arabia suggests the occurrence of multiple zoonotic spillover events (11, 12).

Similarly to severe acute respiratory syndrome coronavirus (SARS-CoV), another *Betacoronavirus* which caused the SARS

pandemic, MERS-CoV appears to target primarily the lower respiratory tract, causing acute respiratory distress in severe human cases (2, 13, 14). However, in contrast to SARS-CoV, which uses angiotensin-converting enzyme 2 (ACE2) as its cellular host receptor (15), MERS-CoV utilizes dipeptidyl peptidase 4 (DPP4; also known as CD26) (16). Interaction of the receptor binding domain (RBD) of the MERS-CoV spike protein with DPP4 initiates attachment to the host cell and subsequent virus internalization. The RBD was mapped to be a 231-amino-acid region in the

S1 subunit of the spike protein (17). DPP4 is a type II transmembrane glycoprotein, involved in cleavage of dipeptides and degradation of incretins (18). DPP4 is widely expressed in different tissues, such as lungs and kidney, and the cells of the immune system, although a detailed description of DPP4 expression in the human respiratory tract and kidney is currently not available. DPP4 is relatively conserved between mammalian species, allowing the MERS-CoV spike protein to bind to both bat and human DPP4 (16, 18).

In vitro studies using a variety of different primary and immortalized cell lines reported a broad tropism of MERS-CoV (19–22). Most cell lines with a human, bat, nonhuman primate, or swine origin were found to be susceptible to infection with MERS-CoV. In contrast, cell lines originating from mice, hamsters, dogs, and cats were not susceptible to MERS-CoV infection (16, 19). *In vitro* data on the species tropism of MERS-CoV appears to correlate with the *in vivo* host restriction of MERS-CoV; rhesus macaques can be experimentally infected with MERS-CoV, whereas inoculation of other commonly used animal models such as the Syrian hamster, mouse, or ferret did not result in efficient viral replication (23–27). Recent studies suggest that DPP4 plays an important role in the nonsusceptibility of the mouse and ferret to MERS-CoV (28–30).

Here, we investigated the host species restriction of MERS-CoV and the role of the DPP4 receptor in this observed species tropism. Differences in DPP4 between MERS-CoV permissive and nonpermissive species were identified to be responsible for the ability of DPP4 to function as the MERS-CoV receptor.

MATERIALS AND METHODS

Biosafety statement. All infectious work with MERS-CoV was performed in a high-containment facility at the Rocky Mountain Laboratories (RML), Division of Intramural Research (DIR), National Institute of Allergy and Infectious Diseases (NIAID), National Institutes of Health (NIH). The work was approved by the RML Institutional Biosafety Committee (IBC) at biosafety level 3 (BSL3).

Ethics statement. Fresh animal tissues were obtained from local slaughter facilities (cow, goat, and sheep) or from an in-house tissue repository (rhesus macaque and mouse) or collected under a tissue sampling protocol (hamster and ferret) approved by the Institutional Animal Care and Use Committee of the Rocky Mountain Laboratories, and the collection was performed following the guidelines of the Association for Assessment and Accreditation of Laboratory Animal Care, International (AAALAC), by certified staff in an AAALAC-approved facility.

Cells and virus. Huh-7 (human carcinoma), Vero (African green monkey kidney), baby hamster kidney (BHK), and mouse embryonic fibroblast (MEF) 3T3 and C57Bl6 cells were maintained in Dulbecco's modified Eagle's medium (DMEM) supplemented with 10% fetal bovine serum (FBS), 2 mM L-glutamine, 50 U/ml penicillin, and 50 μg/ml streptomycin (culture DMEM). Primary ferret kidney cells were generated as follows: within 30 min of tissue collection, the fibrous capsule, adjacent medulla, and any fat, blood clots, and connective tissue were dissected from the ferret kidney, which was subsequently cut into small pieces. The tissue sample was washed with ice-cold Hanks' balanced salt solution (HBSS) containing 10 mM EGTA until the supernatant was clear and further cut into 1-mm³ pieces. Here, the tissue sample was incubated at 37°C for 20 min while it was rolled in 25 ml of warm nonsupplemented DMEM-F12 GlutaMAX medium containing 1 mg/ml collagenase (Worthington) and passed through a 100-μm sieve, a 70-μm sieve, and a 40-μm sieve. Supernatant was centrifuged at 400 × *g* for 5 min at 4°C and washed 3 times with HBSS. The pellet was then resuspended in DMEM-F12 GlutaMAX medium supplemented with 10% FBS, 50 U/ml penicillin, 50 μg/ml streptomycin, 2.5 μg/ml amphotericin B (Fungizone), and 5
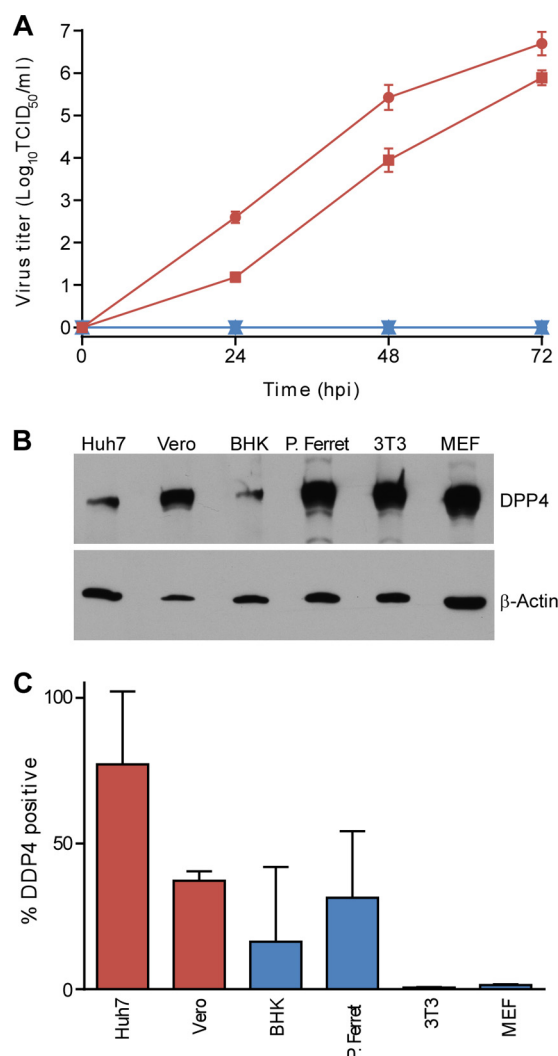

FIG 1 Replication kinetics of MERS-CoV in cell lines of human, nonhuman primate, hamster, mouse, and ferret origin. (A) Huh-7 (red circles), Vero (red squares), BHK (blue circles), 3T3 (blue squares), MEF C57Bl6 (blue triangles), and primary ferret (blue inverted triangles) cell lines were inoculated with MERS-CoV using an MOI of 0.01 TCID$_{50}$/cell. Supernatants were harvested at 0, 24, 48, and 72 h postinoculation (hpi), and viral titers were determined by endpoint titration in quadruplicate in VeroE6 cells. Red lines indicate cell lines originating from species known to be susceptible to MERS-CoV infection; blue lines indicate cell lines originating from species nonsusceptible to MERS-CoV infection. (B) Western blots of cellular lysates of Huh-7, Vero, BHK, primary ferret, 3T3, and MEF C57Bl6 cells probed with anti-DPP4 or anti-actin antibodies. (C) Cells were stained using anti-DPP4 (R&D) and an FITC-conjugated secondary antibody (Life Technologies). Samples were collected using an LSRII flow cytometer (BD Biosciences) and analyzed using FlowJo and GraphPad software. Mean titers were calculated from three independent experiments. Error bars indicate standard deviations.

μg/ml human transferrin (Sigma-Aldrich), and cells were seeded at a density of 5 × 10⁴ cells/cm². The ferret primary kidney cell line was maintained in DMEM-F12 GlutaMAX supplemented with 10% FBS, 50 U/ml penicillin, 50 μg/ml streptomycin, 2.5 μg/ml amphotericin B, and 50 μg/ml human transferrin. All cell lines were maintained at 37°C in 5% CO$_2$. All reagents were purchased from Gibco, unless otherwise specified. MERS-CoV (strain HCoV-EMC/2012) was propagated on VeroE6 cells using DMEM supplemented with 2% FBS, 2 mM L-glutamine, 50 U/ml penicillin, and 50 μg/ml streptomycin (complete DMEM). MERS-CoV
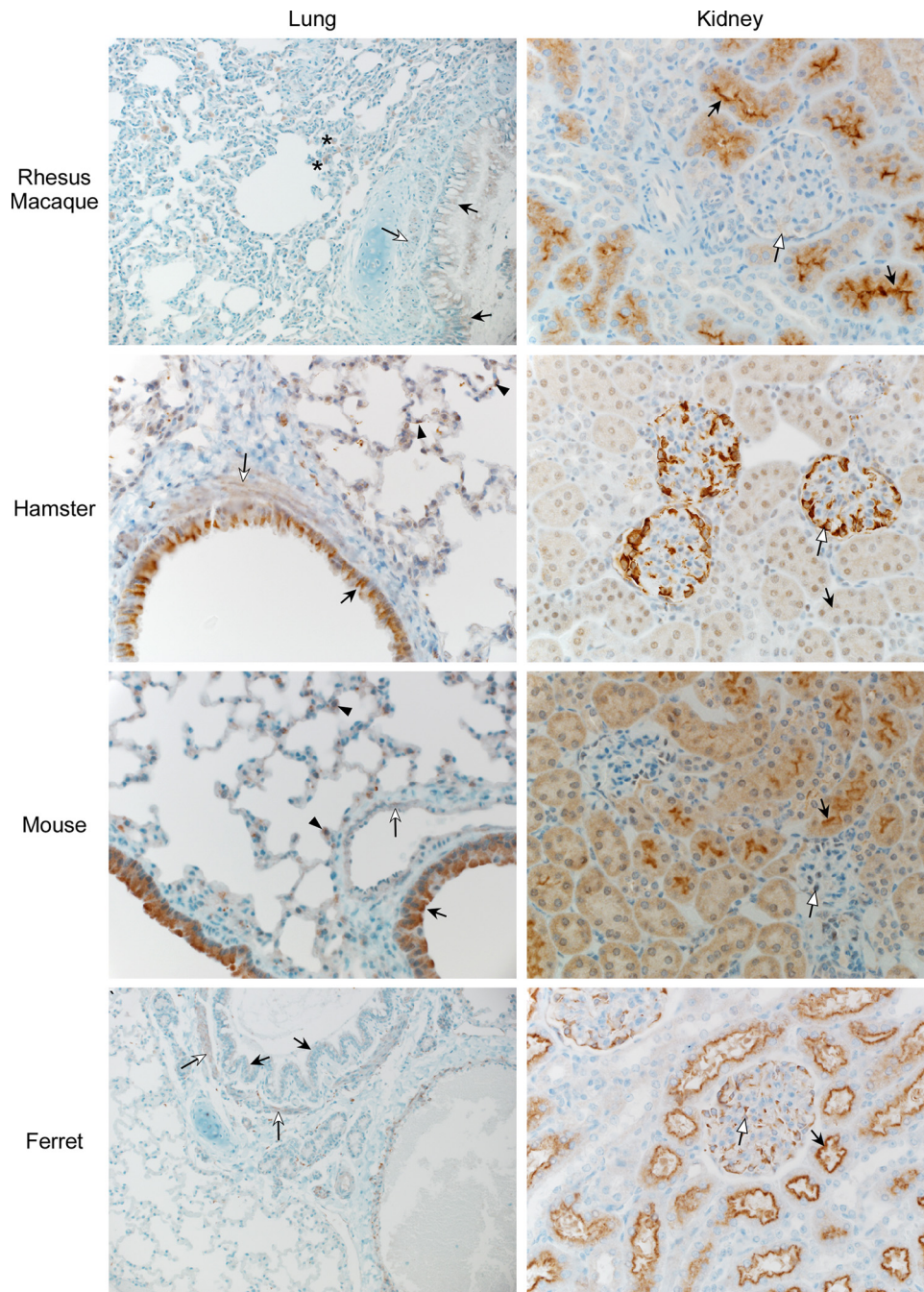
FIG 2 DPP4 in rhesus macaque, hamster, mouse, and ferret lung and kidney tissues. IHC was performed on lung and kidney tissues from rhesus macaque, hamster, mouse, and ferret tissues using an anti-DPP4 antibody. Tissues were fixed in 10% neutral buffered formalin, embedded in paraffin. IHC images, lung: closed arrow, bronchiolar epithelium; open arrow, smooth muscle; asterisk, alveolar macrophage; closed arrowhead, alveolar interstitium. IHC images, kidney: closed arrow, renal tubular epithelium; open arrow, glomerular endothelium (magnification, ×200).

was titrated by endpoint titration in quadruplicate in VeroE6 cells cultured in complete DMEM as follows: cells were inoculated with 10-fold serial dilutions of virus and scored for cytopathic effect 5 days later. Fifty-percent tissue culture infective dose ($TCID_{50}$) was calculated by the method of Spearman-Karber.

DPP4 Western blot analysis. Cells were washed in phosphate-buffered saline (PBS) and lysed in radioimmunoprecipitation (RIPA) buffer (50 mM Tris-HCl [pH 7.5], 150 mM NaCl, 1% NP-40, 0.5% sodium-deoxycholate, 0.1% SDS, and protease inhibitor cocktail tablets [Sigma]).

Lysates were treated with TURBO DNase (Life Technologies). Protein concentrations were determined with the bicinchoninic assay (Thermo Scientific). Cellular lysates were separated on 10% SDS-PAGE gels and transferred to polyvinylidene difluoride (PVDF) membranes (Life Technologies). After being blocked in 5% nonfat milk powder in PBS-0.1% Tween (Fisher Scientific), membranes were incubated overnight with anti-DPP4 rabbit polyclonal antibody (1:700; AbCam; ab28340) or an anti-actin antibody (1:5,000; Sigma-Aldrich; A5441). Membranes were then incubated with a horseradish peroxidase-conjugated anti-rabbit or anti-

TABLE 1 DPP4 expression in lung and kidney tissues of different mammalian species

Tissue or cell type	DPP4 expression[a]							
	Rhesus macaque	Hamster	Mouse	Ferret	Camel	Sheep	Goat	Cow
Lung								
Apical bronchial/bronchiolar epithelium	II	III	IV	I	III	III	II	III
Bronchiolar smooth muscle	I	II	III	III	I	I	I	I
Vascular smooth muscle	I	III	III	II	II	I	II	II
Endothelial cells	I	I	I	0	0	I	II	I
Axonal cells	ND	IV	IV	III	ND	ND	ND	0
Alveolar macrophages	II	I	II	0	I	ND	II	0
Alveolar interstitium	I	II	I	0	0	IV	III	III
Mesothelium	I	I	0	0	0	III	IV	III
Kidney								
Cortical apical proximal tubular epithelium	II	I	II	IV	II	II	II	I
Arteriolar smooth muscle	I	II	I	I	III	II	II	I
Endothelial cells	I	II	0	0	0	II	0	II
Glomerular endothelial cells	I	III	0	III	0	I	II	I
Axonal cells	0	IV	II	IV	ND	I	III	III

[a] The lungs and kidneys of the various species were examined by IHC using an anti-DPP4 antibody. The tissues were evaluated using a scale of 0 to IV based on the intensity of the IHC signal and/or the distribution of antigen throughout the tissue. A score of 0 indicates that no anti-DPP4 staining was detected. I was used when the signal was very weak and/or was found in only a few, scattered cells. II demonstrates a moderate IHC signal in multifocal to diffuse areas within the tissue. III is used to score cells that stained in a moderate to intense fashion in coalescing to diffuse areas. IV indicates intense and diffuse IHC staining in the cells of interest. ND, not detected.

mouse IgG (1:12,500; Jackson ImmunoResearch). Signals were detected with Pierce ECL 2 Western blotting substrate (Thermo Scientific) and developed on blue autoradiography film (GeneMate).

Immunohistochemistry. Immunohistochemistry was performed as described previously (24) using an anti-DPP4 rabbit polyclonal antibody (Abcam; ab28340) at a 1:400 dilution for rhesus macaque, mouse, ferret, sheep, goat, and cow or a 1:800 dilution for hamster and biotinylated anti-rabbit SS link (undiluted; Biogenex; HK336-9R) as a secondary antibody. Tissues were fixed in 10% neutral buffered formalin, embedded in paraffin, and processed for immunohistochemistry using the Discovery XT automated processor (Ventana Medical Systems) with a DapMap kit (Ventana Medical Systems).

Sequencing and cloning of DPP4 sequences. Total RNA from lung and kidney samples from different species was extracted using the RNeasy minikit (Qiagen), and cDNAs were synthesized using random hexamers and SuperScript III reverse transcriptase (Applied Biosystems). Complete DPP4 genes were amplified using iProof high-fidelity DNA polymerase (Bio-Rad) and in-house-designed primers (sequence available upon request).

Plasmids. DPP4 amplicons were sequenced by Sanger sequencing, and sequences were aligned using the MEGA5.2 software package. DPP4 gene sequences for each species were synthesized in expression plasmid pcDNA3.1(+) (GeneArt). Mutagenized DPP4 expression plasmids were generated by synthesizing hamster DPP4 containing five human-specific amino acid residues (Ala291, Ile295, Arg336, Val341, and Ile346; humanized hamster) and human DPP4 containing five hamster-specific amino acid residues (Glu291, Thr295, Thr336, Leu341, and Val346; hamsterized human), flanked by restriction sites BamHI and BsgI (human DPP4) or BamHI and EcoRV (hamster DPP4). Human and hamster DPP4s in pcDNA3.1(+) were restriction digested, purified, and ligated with the humanized hamster or hamsterized human DPP4 fragments, respectively, using T4 DNA ligase (New England Biolabs). Modified DPP4 sequences were confirmed by Sanger sequencing.

Transfection of cells. BHK and primary ferret cells were transfected with 3 μg pcDNA3.1(+) containing the DPP4 genes from different species or pCAGGS-green fluorescent protein (GFP) using 8 μl of Lipofectamine 2000 (Life Technologies). DPP4 expression was confirmed by quantitative reverse transcription-PCR (qRT-PCR) and flow cytometry.

Replication kinetics. Multistep replication kinetics were determined by inoculating cells in triplicate with MERS-CoV with a multiplicity of infection (MOI) of 0.01 (normal cell lines) or 1 (transfected cell lines) $TCID_{50}$ per cell. The lower MOI of 0.01 was chosen for experiments performed to determine the ability of cell lines to support multiple replication cycles of MERS-CoV, whereas the higher MOI of 1 was chosen for cells naturally nonsusceptible for MERS-CoV but with the various DPP4s transiently expressed to maximize the likelihood of the transfected cell to encounter MERS-CoV. One hour after inoculation, cells were washed once with DMEM and fresh medium was placed on the cells. Supernatants were sampled at 0, 24, 48, and 72 h after inoculation, and virus titers in these supernatants were determined as described.

Flow cytometry. Cells were washed with PBS and removed with 5 mM EDTA (BHKs and 3T3s) or spun down from suspension (primary ferret cells, Huh-7 cells, Vero cells, and MEF) and then washed twice, resuspended in PBS with 2% FBS, and stained at 4°C using anti-human DPP4 antibody (R&D; catalog no. AF1180), followed by staining with fluorescein isothiocyanate (FITC)-tagged donkey anti-goat antibody (Life Technologies; catalog no. A-11055). As a control, samples of cells were stained with secondary antibody only. After being stained, cells were washed, resuspended in PBS with 2% FBS, stained with 7-aminoactinomycin D (Life Technologies), and analyzed immediately. Samples were collected using an LSRII flow cytometer (BD Biosciences). Analysis gates were set on viable cells, and 10,000 gated events were analyzed for each sample. Data were analyzed using FlowJo software (TreeStar) comparing transfected cells against untransfected cells.

Binding energy modeling. The DPP4 homology models were constructed using the human DPP4 structure (Protein Data Bank [PDB] identifier [ID] 4KR0, chain A) as the template. The sequence alignment was generated using CLUSTALW2 (31), and the initial model was built using Nest (32) based on the alignment and the human DPP4 structure. The resulting structural model was briefly optimized using the TINKER minimization program "minimize.x" with OPLS all-atom force field and L-BFGS quasi-Newton optimization algorithm (33). For each species, the RBD-DPP4 complex model was generated by merging the RBD domain (PDB ID 4KR0, chain B) with the DPP4 model, which was then subjected to the binding energy calculation using an all-atom distance-dependent pairwise statistical potential, DFIRE (34). The energy difference between the complex and two individual structures, DPP4 and RBD, was taken as the binding energy.

qRT-PCR of DPP4 mRNA expression. Expression of DPP4 mRNA was measured via qRT-PCR. Total RNA was extracted from transfected

homogenized cells using the standard TRIzol-chloroform procedure (Life Technologies), followed by further extraction using the RNeasy minikit (Qiagen) combined with a 30-min on-column DNase I (Qiagen) digestion according to the manufacturer's instructions. mRNA was purified from total RNA via the NucleoTrap mRNA minikit (Macherey-Nagel). One-step qRT-PCR was performed in three separate experiments on the Rotor-GeneQ (Qiagen) for the detection of DPP4 and hypoxanthine phosphoribosyltransferase (HPRT) using the Quantifast probe PCR master mix (Qiagen) according to the manufacturer's instructions. Probes for DPP4 (FAM-AGCTTTGATGGCAGAGGAAGTGGT-BHQ1, where FAM is 6-carboxyfluorescein and BHQ1 is black hole quencher 1) and HPRT (FAM-ACTTTGTTGGATTTGAAATTCCAGACAAGTTTG-BHQ1) were designed using a cross-species high-conservancy region in the gene. Forward and reverse primer sets were species specific (sequences available upon request). Relative fold increase was calculated by the comparative cycle threshold (C_T) method (35), where DPP4 expression is normalized to HPRT.

Nucleotide sequence accession numbers. All newly generated DPP4 nucleotide sequences are available from GenBank under accession numbers KF574262 to KF574268.

RESULTS

Replication kinetics of MERS-CoV in different cell lines. The replication kinetics of MERS-CoV was studied in cells of different mammalian origin: Huh-7 (human), Vero (African green monkey), BHK (hamster), MEF C57Bl6 and 3T3 (mouse), and ferret primary kidney cells. MERS-CoV replicated efficiently in Huh-7 and Vero cells. In contrast, MERS-CoV did not replicate in BHK, MEF C57Bl6 and 3T3, and ferret primary kidney cells (Fig. 1A). These data correspond with the current information on the ability of MERS-CoV to infect humans and nonhuman primates (rhesus macaques [23, 25]) and the inability of MERS-CoV to infect mice, hamsters, and ferrets (24, 26, 27). The presence of the MERS-CoV receptor, DPP4, is essential in the initiation of infection. To investigate whether the lack of infection by MERS-CoV of nonsusceptible cell lines was due to a lack of expression of the DPP4 receptor, we performed Western blot analyses. DPP4 protein was detected in cell lines both permissive and nonpermissive for MERS-CoV infection although not uniformly found to be expressed on the cell surface (Fig. 1B and C).

Detection of DPP4 in tissues. To determine the cell types in which DPP4 was expressed in the lungs and kidney of rhesus macaque, hamster, mouse, and ferret, immunohistochemistry (IHC) was performed using an anti-DPP4 antibody. In both the lungs and kidneys of the investigated species, DPP4 was found to be present. In the lungs, DPP4 was abundantly present on bronchiolar epithelium cells and occasionally present on alveolar interstitium, or absent in the case of ferrets (Fig. 2, Table 1). The intensity of the anti-DPP4 staining of bronchiolar epithelium ranged from weak in ferrets to moderate in the macaque and hamster and very intense in the mouse. All species tested, except the ferret, also demonstrated weak anti-DPP4 immunoreactivity at the level of alveoli. The kidney tissue was similar to lung tissue in that all species demonstrated anti-DPP4 immunoreactivity to epithelial cells. The intensity of staining was again variable, with weak staining in the hamster, moderate staining in the macaque and mouse, and intense staining in the ferret. DPP4 was present on kidney vascular smooth muscle cells, with weak staining in the macaque, mouse, and ferret and moderate staining in the hamster. All species except the mouse displayed the presence of DPP4 on either glomerular or vascular endothelium, with the strongest staining seen in the glomeruli of hamsters and ferrets.

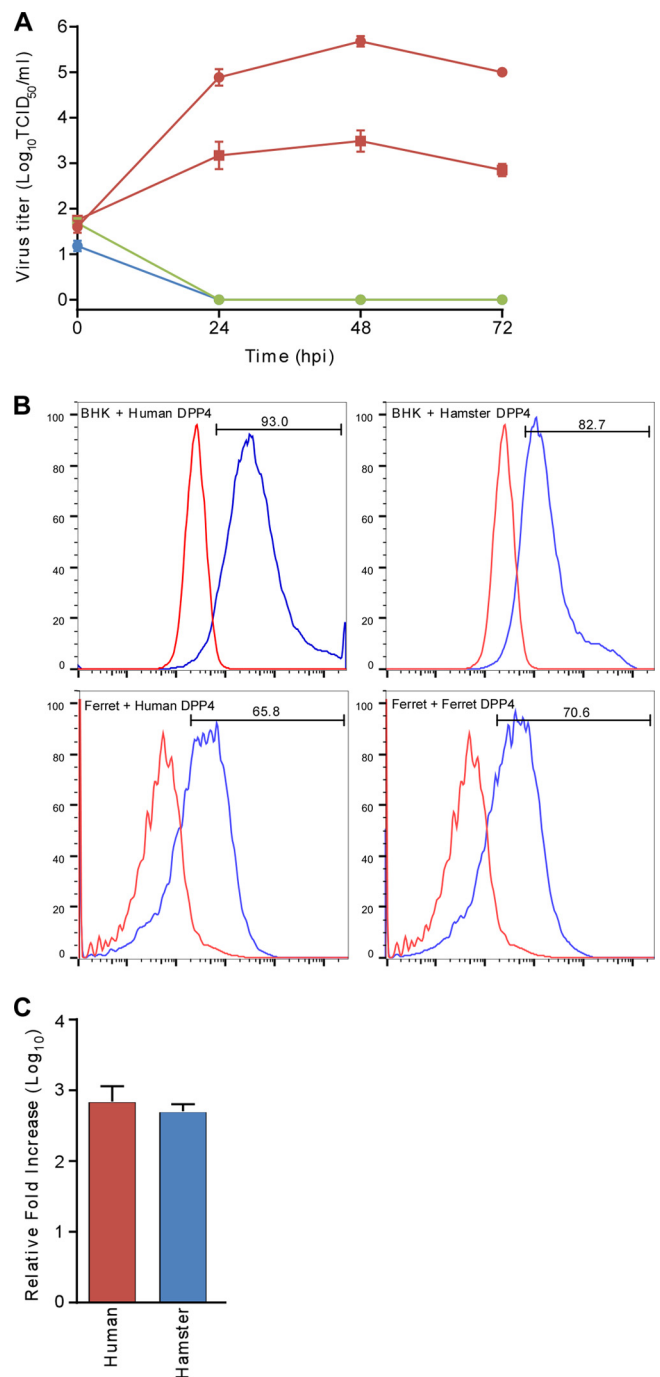The presence of DPP4 in cell lines nonsusceptible to MERS-

FIG 3 Replication kinetics of MERS-CoV on hamster and ferret cell lines expressing human, hamster, or ferret DPP4. (A) Human DPP4 (red), hamster DPP4 (blue), ferret DPP4 (blue), and GFP (green) were expressed in BHK (circles) or primary ferret (squares) cells. Twenty-four hours posttransfection, cells were inoculated with MERS-CoV using an MOI of 1 $TCID_{50}$/cell. Supernatants were harvested at 0, 24, 48, and 72 hpi, and viral titers were determined by endpoint titration in quadruplicate in VeroE6 cells. Mean titers were calculated from three independent experiments. Error bars indicate standard deviations. (B) BHK or primary ferret cells were left untransfected (red) or transfected with DPP4 (blue) and stained 24 h posttransfection using anti-DPP4 (R&D) and an FITC-conjugated secondary antibody (Life Technologies). Samples were collected using an LSRII flow cytometer (BD Biosciences) and analyzed using FlowJo software. (C) Expression of DPP4 mRNA was measured via qRT-PCR. Relative fold increase was calculated by the comparative C_T method (35), where DPP4 expression is normalized to HPRT.

TABLE 2 Alignment of DPP4 amino acid residues of different mammalian species interacting with the MERS-CoV spike protein[a]

Species	Amino acid residue (human DPP4 numbering)													
	229	267	286	288	291	294	295	298	317	322	336	341	344	346
Human	N	K	Q	T	A	L	I	H	R	Y	R	V	Q	I
Hamster					E		T				T	L		V
Rhesus macaque														
Mouse				P		A	R				T	S		V
Ferret		E		D		S	T	Y			S	E	E	T
Camel			V											
Sheep			V		G									
Cow			V		G									
Goat			V		G									

[a] Full DPP4 protein sequences were compared using MegAlign software.

CoV and on cells in the respiratory tract of nonpermissive species (mouse, hamster, and ferret) suggests that the inability of MERS-CoV to replicate in these species is either due to an inability of the MERS-CoV spike protein to bind to the respective DPP4s or an incompatibility of MERS-CoV with the cellular machinery of these respective species.

Specificity of MERS-CoV spike protein for DPP4. The DPP4 coding sequences of human, hamster, and ferret, obtained from GenBank or by sequencing, were cloned into expression vector pcDNA3.1(+) and transfected into cell lines nonsusceptible to MERS-CoV replication. The expression of DPP4 on transfected cells was determined by qRT-PCR and flow cytometry (Fig. 3B and C). Transient expression of human DPP4 in BHK and primary ferret kidney cells allowed these previously nonsusceptible cells to support MERS-CoV replication, whereas transient expression of hamster DPP4 in BHK cells, ferret DPP4 in ferret primary cells, or GFP in either cell type did not render these cells susceptible to MERS-CoV replication (Fig. 3A). As surface expression of human DPP4, but not hamster or ferret DPP4, allowed MERS-CoV replication in previously nonsusceptible cell lines, the observed MERS-CoV species tropism is most likely a result of the inability of its spike protein to bind to hamster or ferret DPP4 rather than the incompatibility of MERS-CoV with the hamster or ferret cellular machinery.

Structural modeling of MERS-CoV receptor binding domain with multispecies DPP4. Recent cocrystallization studies of the MERS-CoV spike protein and the human DPP4 identified 14 amino acids in DPP4 important in binding to the MERS-CoV spike protein (36, 37). Alignment of the DPP4 amino acid sequences of human and hamster origin revealed a total of five differences within these 14 amino acids (Table 2). To investigate the binding potential of the different DPP4s to MERS-CoV spike protein, DPP4 homology models were built using the human DPP4 structure (PDB ID 4KR0, chain A) as a template (36). Of the five amino acid residues at the RBD interface that differ between human and hamster DPP4, the residues at positions 291 and 336 appear to be most critical for the species specificity. In the human DPP4-RBD crystal structure, the small methyl side chain of Ala291 in DPP4 nestles into a small pocket in the RBD, which cannot accommodate the size and charge of the corresponding glutamic acid residue found in the hamster DPP4 molecule. This steric clash alone is likely sufficient to abrogate binding. In addition, the side chain of Arg336 in human DPP4 forms hydrogen bonds with RBD residue Tyr499 and a salt bridge to RBD residue Asp455. These interactions would not be formed by the corre-

sponding threonine side chain in hamster DPP4. The remaining three DPP4 residues at the RBD interface that differ in humans and hamsters are conserved substitutions and are not predicted to greatly impact binding to the RBD (Fig. 4A). Furthermore, these analyses showed that hamster DPP4 has significantly higher binding energy (less favorable interactions) than human DPP4 to MERS-CoV (Fig. 4B). When mutant DPP4s were designed *in silico* by introducing the five human-specific amino acid residues (Ala291, Ile295, Arg336, Val341, and Ile346) into the hamster DPP4 (humanized hamster DPP4) and the five hamster-specific amino acid residues (Glu291, Thr295, Thr336, Leu341, and Val346) into the human DPP4 (hamsterized human DPP4), a reversion of the binding energies was found; the binding energy associated with the humanized hamster DPP4 and MERS-CoV spike protein complex was lower than that of hamsterized human DPP4 and MERS-CoV spike protein (Fig. 4B). This suggests that the five DPP4 human-specific amino acid residues are responsible for the ability of MERS-CoV spike protein to bind to DPP4.

***In vitro* characterization of mutagenized DPP4s.** The modeling data suggested that introduction of the five human-specific amino acid residues in hamster DPP4 would allow recognition of this DPP4 by the MERS-CoV spike protein. To test this hypothesis, expression plasmids were synthesized with human DPP4 containing the five hamster-specific amino acid residues (hamsterized human DPP4) and hamster DPP4 containing the five human-specific amino acid residues (humanized hamster DPP4). Inoculation of BHK cells transiently expressing humanized hamster DPP4 with MERS-CoV resulted in virus replication, whereas inoculation of BHK cells transiently expressing hamsterized human DPP4 did not (Fig. 5A). Expression of DPP4 on BHK cells was confirmed via flow cytometry (Fig. 5B).

Modeling and *in vitro* characterization of the DPP4 of putative intermediate host species. We determined the binding energy of DPP4s to MERS-CoV spike protein of known binders (rhesus macaque) and nonbinders (ferret and mouse). Like hamster DPP4, the binding energy of ferret and mouse DPP4 to MERS-CoV spike protein was found to be relatively high. In contrast, rhesus macaque DPP4 was found to have binding energy levels similar to human DPP4 (Fig. 4B). These results were confirmed *in vitro* by transfecting BHK cells with DPP4 from rhesus macaque and subsequently inoculating these cells with MERS-CoV, resulting in virus replication. In contrast, transfection of the DPP4 of ferret or mouse origin into BHK cells did not render these cells susceptible to MERS-CoV replication (Fig. 6). With the identification of dromedary camels as a potential intermediate host
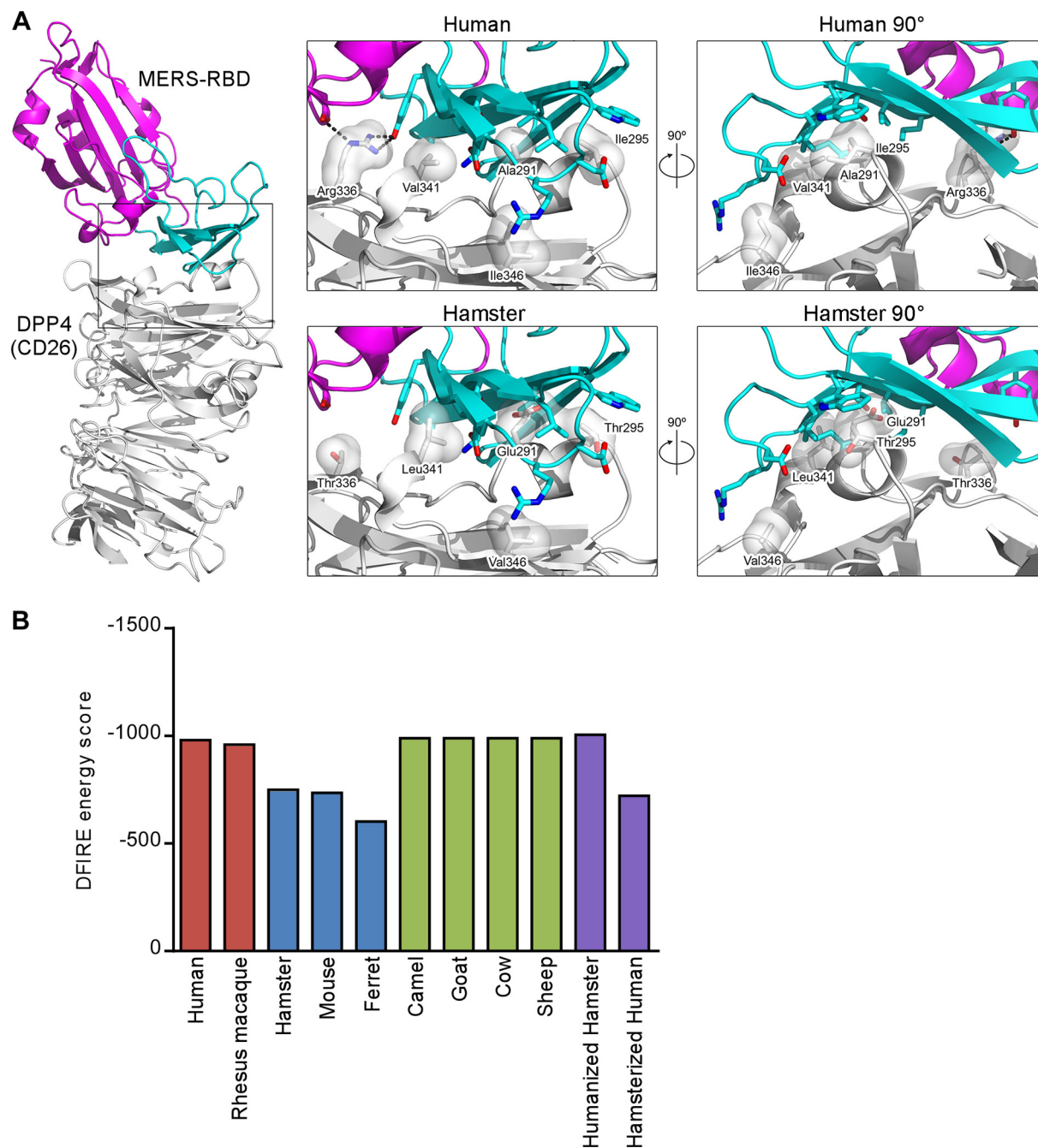
FIG 4 Interaction between MERS-CoV spike protein and DPP4s of different mammalian species. (A) Cartoon representing the binding between human DPP4 or hamster DPP4 and the spike protein of MERS-CoV. DPP4 is depicted in white; the receptor binding domain (RBD) of the spike protein of MERS-CoV is depicted in magenta and cyan. The far right panel is obtained by clockwise rotation of the middle panel along a longitudinal axis. (B) Binding energies between spike protein of MERS-CoV and DPP4 of different species as well as humanized hamster DPP4 and hamsterized human DPP4. Red bars indicate the binding energies of known binders (human and rhesus macaque DPP4), blue bars indicate the binding energies of nonbinders (hamster, mouse, and ferret DPP4), green bars indicate the binding energies of unknown binders (dromedary camel, goat, cow, and sheep), and purple bars indicate the binding energies of the *in silico* mutagenized hamster and human DPP4s. The DPP4 homology models were constructed using the human DPP4 structure (PDB ID 4KR0, chain A) as a template and subjected to the binding energy calculation using an all-atom distance-dependent pairwise statistical potential, DFIRE.

species for MERS-CoV in mind, we determined the ability of DPP4 from putative intermediate host species (dromedary camel, cow, sheep, and goat) to bind to MERS-CoV spike protein. Like DPP4 from human and rhesus macaque, the binding energy associated with dromedary camel, goat, sheep, and cow DPP4 was

found to be relatively low, suggesting these proteins can function as a receptor for MERS-CoV (Fig. 4B). Furthermore, expression of dromedary camel, goat, sheep, and cow DPP4 on BHK cells supported replication of MERS-CoV (Fig. 6A). Expression of DPP4 on BHK cells was confirmed via flow cytometry and qRT-PCR
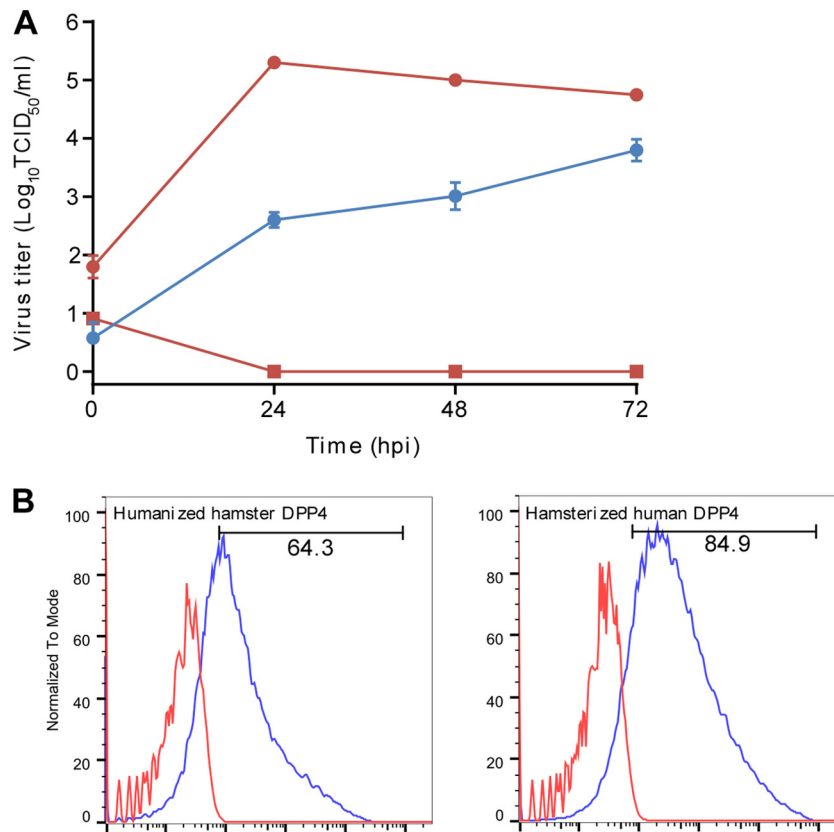
FIG 5 Replication kinetics of MERS-CoV on BHK cells expressing mutagenized DPP4s. (A) Humanized hamster DPP4 (blue circles) or hamsterized human DPP4 (red squares) was expressed on BHK cells. As a control, human DPP4 (red circles) was expressed on BHK cells. Twenty-four hours posttransfection, cells were inoculated with MERS-CoV using an MOI of 1 TCID$_{50}$/cell. Supernatants were harvested at 0, 24, 48, and 72 hpi, and viral titers were determined by endpoint titration in quadruplicate in VeroE6 cells. Mean titers were calculated from three independent experiments. Error bars indicate standard deviations. (B) BHK cells were left untransfected (red) or transfected with DPP4 (blue) and stained 24 h posttransfection using anti-DPP4 (R&D) and an FITC-conjugated secondary antibody (Life Technologies). Samples were collected using an LSRII flow cytometer (BD Biosciences) and analyzed using FlowJo software.

(Fig. 6B and C). DPP4 was detected on cells in the lung and kidney tissue of camel, goat, cow, and sheep by IHC. Interestingly, DPP4 was more abundantly expressed on alveolar interstitium in cow, goat, and sheep lungs compared to in dromedary camel, rhesus macaque, hamster, mouse, and ferret lungs (Fig. 7, Table 1). Finally, we carried out full-length and partial (DPP4 binding domain, amino acids 220 to 350) protein sequence alignments between the DPP4 of camel, goat, cow, and sheep. Camel DPP4 diverged from goat, cow, and sheep DPP4, in particular when comparing partial DPP4 protein sequences (Table 3).

DISCUSSION

Surface receptors play an essential role in initiating virus entry into the host cell, thereby playing a major role in the tissue and host species tropism of viruses. DPP4 was recently identified as the cellular receptor for MERS-CoV (16). Based on the ability of MERS-CoV to replicate in cell lines originating from a wide variety of mammalian species (bats, nonhuman primates, pigs, and humans), it was speculated to have a broad host tropism (19, 21). However, it is currently unclear whether *in vitro* results correlate directly with *in vivo* susceptibility (38). MERS-CoV was found to be unable to infect some of the major respiratory animal models (Syrian hamster, mouse, and ferrets [24, 26, 27]), in contrast to the ability of MERS-CoV to replicate efficiently in rhesus macaques

(23). This suggests the existence of a host-barrier restriction of MERS-CoV for some species. Using *in vitro* growth kinetics of MERS-CoV, we were able to demonstrate this host species restriction in cell lines from different mammalian origins. MERS-CoV replicated efficiently in cells of human and nonhuman primate origin but was not able to replicate in cells of mouse, hamster, or ferret origin, despite the presence of DPP4 (Fig. 1). Analysis of the presence of DPP4 in Syrian hamster, mouse, and ferret lung and kidney tissues as well as the rhesus macaque lung and kidney tissues suggested that the inability of MERS-CoV to infect Syrian hamster, mouse, and ferret is not due to a lack of expression of the DPP4 receptor (Fig. 2). Our hypothesis that the host species restriction of MERS-CoV lies on the receptor binding level was supported by the lack of replication in hamster and ferret cells upon exogenous expression of the hamster or ferret DPP4 on the surface of these cells, whereas expression of the human DPP4 receptor rendered these previously nonpermissive cell lines permissive for MERS-CoV (Fig. 3). We observed a >2 log difference in growth of MERS-CoV between hamster and ferret cells, which may be explained by the difference in transfection efficiency (BHKs, 93.0%; primary ferret cells, 65.8%; Fig. 3B). The cocrystallization between the human DPP4 and the MERS-CoV spike protein revealed the receptor binding domain of MERS-CoV and the amino acid residues of human DPP4 interacting with this domain (36, 37). Align-
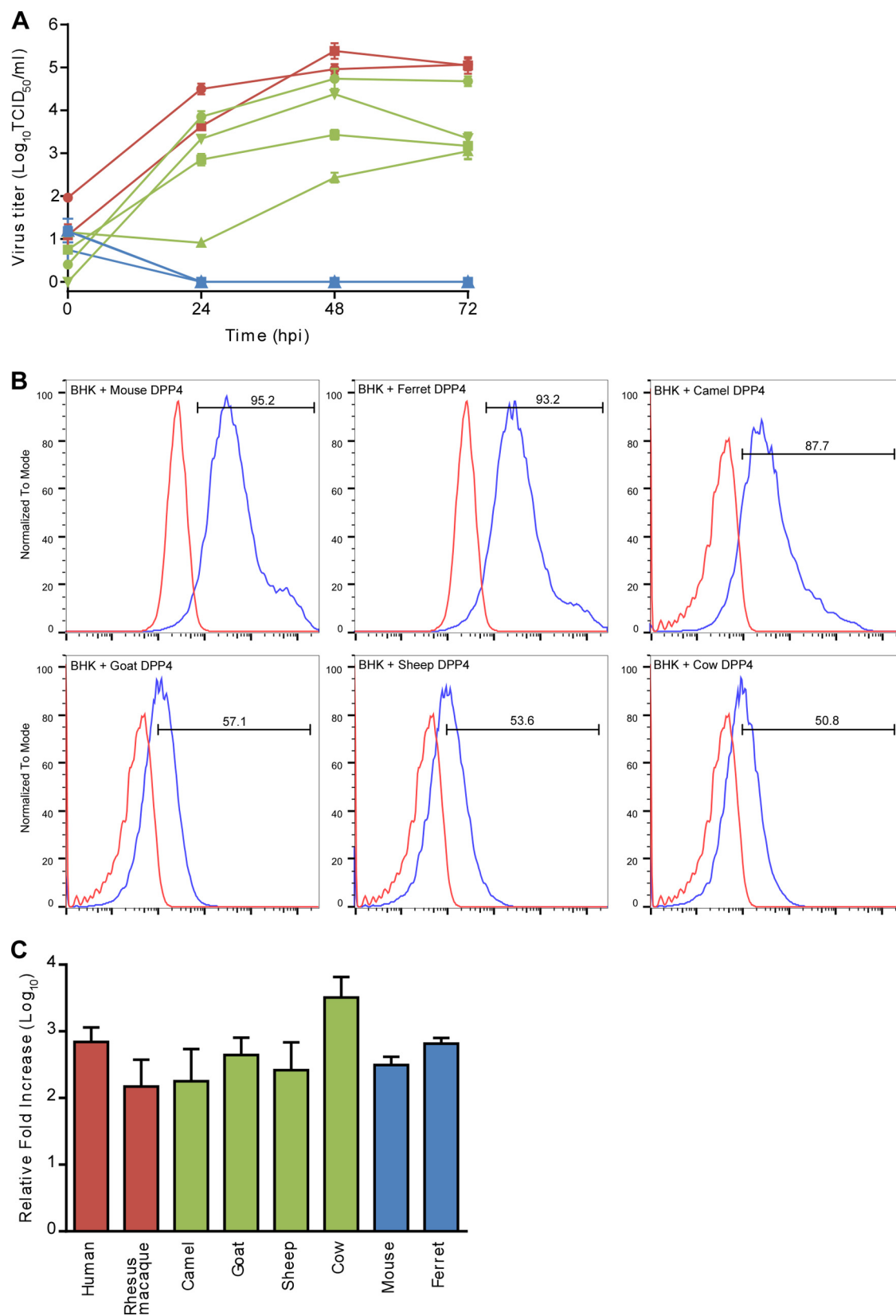
FIG 6 Replication kinetics of MERS-CoV on BHK cells expressing DPP4 of livestock species. Camel (green circles), cow (green squares), goat (green triangles), or sheep (green inverted triangles) DPP4 and rhesus macaque (red squares), ferret (blue squares), or mouse (blue triangles) DPP4 were expressed on BHK cells. As a control, human (red) or hamster (blue) DPP4 was expressed on BHK cells. Twenty-four hours posttransfection, cells were inoculated with MERS-CoV using an MOI of 1 $TCID_{50}$/cell. Supernatants were harvested at 0, 24, 48, and 72 hpi, and viral titers were determined by endpoint titration in quadruplicate in VeroE6
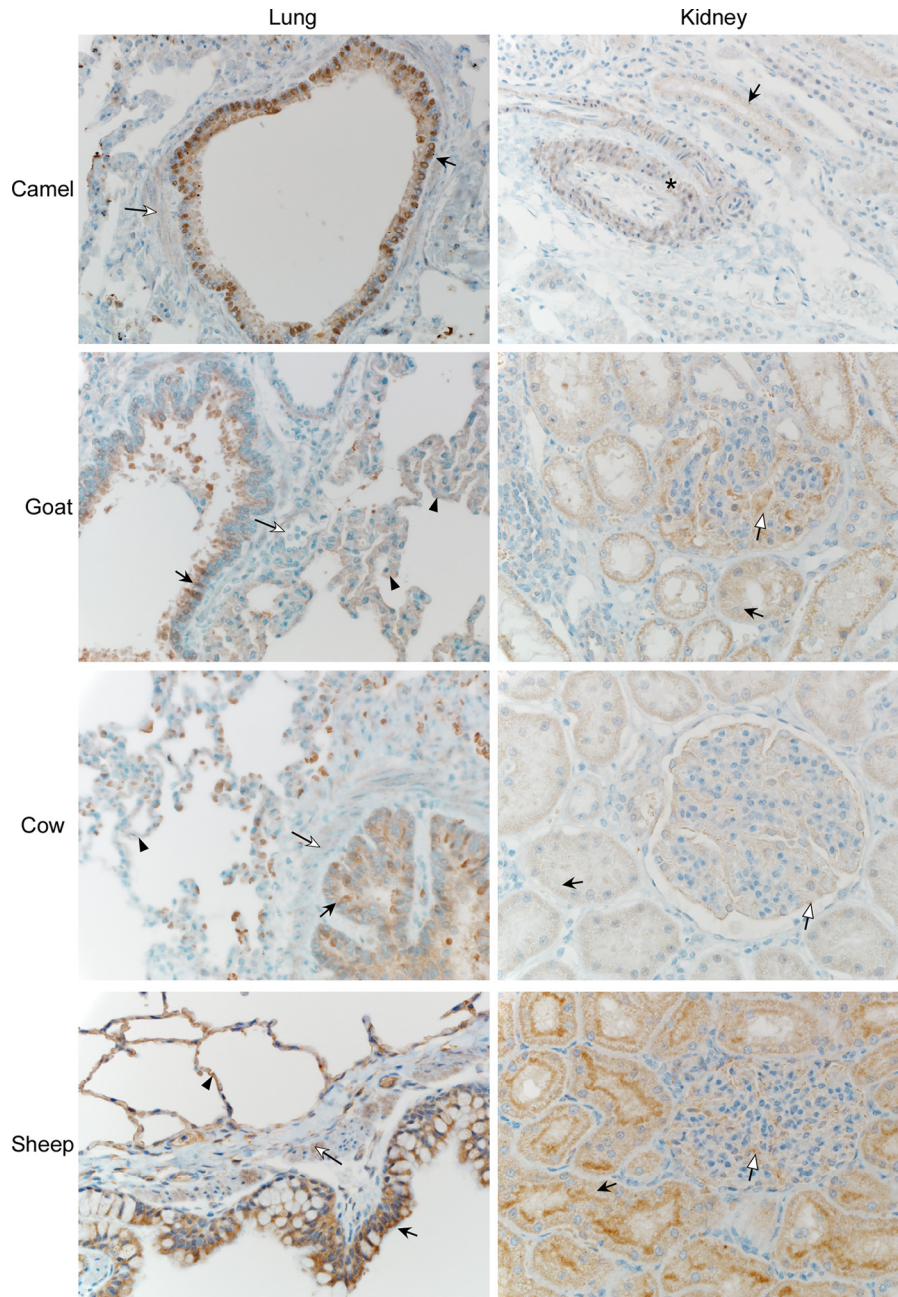
FIG 7 DPP4 in camel, goat, cow, and sheep lung and kidney tissue. IHC was performed on lung and kidney tissues from camel, goat, cow, and sheep using an anti-DPP4 antibody. Tissues were fixed in 10% neutral buffered formalin, embedded in paraffin. IHC images, lung: closed arrow, bronchiolar epithelium; open arrow, smooth muscle; asterisk, alveolar macrophage; closed arrowhead, alveolar interstitium. IHC images, kidney: closed arrow, renal tubular epithelium; open arrow, glomerular endothelium (magnification, ×200).

ment of DPP4 amino acid residues identified as interacting with the MERS-CoV spike protein between human and rhesus DPP4s (binders) and hamster DPP4 (nonbinder) revealed a minimal subset of five amino acid changes between the human and the hamster DPP4 (Table 2). These five differential human amino acid residues were introduced into the hamster DPP4 (humanized hamster DPP4), and the five differential hamster amino acid residues were introduced into the human DPP4 (hamsterized human

cells. Mean titers were calculated from three independent experiments. Error bars indicate standard deviations. (B) BHK cells were left untransfected (red) or transfected with DPP4 (blue) and stained 24 h posttransfection using anti-DPP4 (R&D) and an FITC-conjugated secondary antibody (Life Technologies). Samples were collected using an LSRII flow cytometer (BD Biosciences) and analyzed using FlowJo software. (C) Expression of DPP4 mRNA was measured via qRT-PCR. Relative fold increase was calculated by the comparative C_T method (35), where DPP4 expression is normalized to HPRT.

TABLE 3 Percent identity between DPP4 protein sequences

Animals with partial DPP4 sequences	% identity with animals with full DPP4 sequences[a]			
	Camel	Goat	Cow	Sheep
Camel		91.6	91.6	91.5
Goat	88.5		98.4	99.3
Cow	88.5	100		98.2
Sheep	88.5	100	100	

[a] Full DPP4 and partial (amino acids 220 to 350) DPP4 protein sequences were compared, and percent identities were analyzed using MegAlign software.

DPP4). Expression of the humanized hamster DPP4 in BHK cells rendered these cells permissive for MERS-CoV, whereas expression of hamsterized human DPP4 did not change the nonpermissiveness of the cells (Fig. 5). For ferret DPP4, it was recently shown that exchanging the amino acid region 246 to 505 with that of human DPP4 resulted in the ability of MERS-CoV to utilize this chimeric DPP4 (28), as was the case for mouse DPP4 when exchanging amino acids 279 to 346 with the human DPP4 counterpart (29). In addition, both of these studies found amino acids to be important in spike binding that were identified in this study (295, 336, and 346 for mouse and 295, 336, and 341 for ferret) (28, 29). Interestingly, although the humanized hamster DPP4 was able to facilitate MERS-CoV infection, MERS-CoV titers were considerably lower. This could indicate that although substitution of five human amino acids into hamster DPP4 is sufficient for spike binding, additional amino acid residues in the interface might be required for optimal binding and infectivity.

Currently, the only available animal disease model for MERS-CoV is the rhesus macaque. Research into therapeutic and prophylactic countermeasures is severely restricted by the absence of a small animal model allowing high-throughput *in vivo* screening of antivirals with *in vitro* efficacy or candidate vaccines (24, 25, 39–42). Our data indicate that transgenic mice expressing the human DPP4 will likely be susceptible to MERS-CoV and would allow the establishment of a much-needed small-animal model. This is supported by recent experimental evidence which showed that transient expression of human DPP4 in the lower respiratory tract of mice supported MERS-CoV replication (43).

Subsequent modeling between DPP4s of species known to be able to bind MERS-CoV spike protein (human and rhesus macaque) and species known not to be able to bind MERS-CoV spike protein (hamster, mouse, and ferret) displayed a stark difference in binding energies between binders and nonbinders. Utilizing the same model, DPP4s of species implicated in the emergence of MERS-CoV (dromedary camel, sheep, goat, and cow) were predicted to be able to bind to the spike protein of MERS-CoV (Fig. 4B). DPP4 modeling data were supported by experimental work showing that indeed the DPP4s of dromedary camel, sheep, goat, and cow were able to support MERS-CoV replication (Fig. 6). MERS-CoV-like antibodies have been found in dromedary camels but not yet in goat, sheep, or cow species (7, 44). However, DPP4 from goat, cow, and sheep can function as a receptor for MERS-CoV, although with lesser efficiency (Fig. 6). Protein sequence alignments of full-length and partial DPP4 revealed that camel DPP4 differs from goat, cow, and sheep DPP4, in particular when amino acids 220 to 350 of DPP4, which are of importance in spike binding, were investigated (Table 3). It is possible that subtle dif-

ferences in binding of spike and DPP4 account for the apparent lack of MERS-CoV circulation in the goat, cow, and sheep population. The close evolutionary relationship between MERS-CoV and bat CoVs as well as the detection of a short fragment of viral RNA in a bat in Saudi Arabia suggest that MERS-CoV originates from bats (1, 3). The ability of MERS-CoV to utilize the DPP4 from an insectivorous bat underlines the broad host range (16). Future receptor binding and experimental infection studies are needed to investigate the suitability of different bat species to function as a host for MERS-CoV.

MERS-CoV was found to replicate predominantly in type I and II pneumocytes in the lower respiratory tract of experimentally infected rhesus macaques. The replication of MERS-CoV correlates with DPP4 expression on type I and II pneumocytes in the lungs of rhesus macaques (Fig. 2) (25). The presence of DPP4 in the lower respiratory tract of dromedary camel, sheep, goat, and cow (Table 1) suggests that the tropism of MERS-CoV for these species could be similar to the respiratory tropism observed in rhesus macaques and humans (13, 14, 25). Since the first emergence of MERS-CoV in 2012, the epidemiology has remained unclear. The recent identification of the circulation of MERS-CoV in dromedary camels (6–9) together with the multiple introductions of MERS-CoV into the human population (11, 12) suggests that both zoonotic transmission from an intermediate host and human-to-human transmission occur simultaneously. Our data support the potential for the existence of one or multiple natural reservoirs for MERS-CoV. Although our data do not provide any formal proof for the existence of such a reservoir, the ability of DPP4s of cows, sheep, goats, and dromedary camels (the major Middle East livestock species) to function as a MERS-CoV receptor and the abundant DPP4 presence in the respiratory tract of these species suggest that they would be susceptible for MERS-CoV infection. The combination of modeling the binding energies of the MERS-CoV spike with the DPP4s of different species and a molecular experimental approach could guide field programs focused at identifying the existence of an intermediate host. With the potential susceptibility of major livestock species for MERS-CoV, renewed focus should be aimed at elucidating the existence of an intermediate host and thereby preventing further spread of MERS-CoV.

REFERENCES

1. **Zaki AM, van Boheemen S, Bestebroer TM, Osterhaus AD, Fouchier RA.** 2012. Isolation of a novel coronavirus from a man with pneumonia in Saudi Arabia. N. Engl. J. Med. **367:**1814–1820. http://dx.doi.org/10.1056/NEJMoa1211721.
2. **WHO.** 2013. Coronavirus infections. World Health Organization, Geneva, Switzerland. http://www.who.int/csr/don/archive/disease/coronavirus_infections/en/index.html.
3. **Memish ZA, Mishra N, Olival KJ, Fagbo SF, Kapoor V, Epstein JH, Alhakeem R, Durosinloun A, Al Asmari M, Islam A, Kapoor A, Briese**

T, Daszak P, Al Rabeeah AA, Lipkin WI. 2013. Middle East respiratory syndrome coronavirus in bats, Saudi Arabia. Emerg. Infect. Dis. http://dx.doi.org/10.3201/eid1911.131172.

4. Ithete NL, Stoffberg S, Corman VM, Cottontail VM, Richards LR, Schoeman MC, Drosten C, Drexler JF, Preiser W. 2013. Close relative of human Middle East respiratory syndrome coronavirus in bat, South Africa [letter]. Emerg. Infect. Dis. http://dx.doi.org/10.3201/eid1910.130946.

5. Annan A, Baldwin HJ, Corman VM, Klose SM, Owusu M, Nkrumah EE, Badu EK, Anti P, Agbenyega O, Meyer B, Oppong S, Sarkodie YA, Kalko EK, Lina PH, Godlevska EV, Reusken C, Seebens A, Gloza-Rausch F, Vallo P, Tschapka M, Drosten C, Drexler JF. 2013. Human betacoronavirus 2c EMC/2012-related viruses in bats, Ghana and Europe. Emerg. Infect. Dis. 19:456–459. http://dx.doi.org/10.3201/eid1903.121503.

6. Reusken CB, Haagmans BL, Muller MA, Gutierrez C, Godeke GJ, Meyer B, Muth D, Raj VS, Vries LS, Corman VM, Drexler JF, Smits SL, El Tahir YE, De Sousa R, van Beek J, Nowotny N, van Maanen K, Hidalgo-Hermoso E, Bosch BJ, Rottier P, Osterhaus A, Gortazar-Schmidt C, Drosten C, Koopmans MP. 2013. Middle East respiratory syndrome coronavirus neutralising serum antibodies in dromedary camels: a comparative serological study. Lancet Infect. Dis. 13:859–866. http://dx.doi.org/10.1016/S1473-3099(13)70164-6.

7. Perera RA, Wang P, Gomaa MR, El-Shesheny R, Kandeil A, Bagato O, Siu LY, Shehata MM, Kayed AS, Moatasim Y, Li M, Poon LL, Guan Y, Webby RJ, Ali MA, Peiris JS, Kayali G. 2013. Seroepidemiology for MERS coronavirus using microneutralisation and pseudoparticle virus neutralisation assays reveal a high prevalence of antibody in dromedary camels in Egypt, June 2013. Euro Surveill. 18(36):pii=20574. http://www.eurosurveillance.org/ViewArticle.aspx?ArticleId=20574.

8. Haagmans BL, Al Dhahiry SH, Reusken CB, Raj VS, Galiano M, Myers R, Godeke GJ, Jonges M, Farag E, Diab A, Ghobashy H, Alhajri F, Al-Thani M, Al-Marri SA, Al Romaihi HE, Al Khal A, Bermingham A, Osterhaus AD, Alhajri MM, Koopmans MP. 2014. Middle East respiratory syndrome coronavirus in dromedary camels: an outbreak investigation. Lancet Infect. Dis. 14:140–145. http://dx.doi.org/10.1016/S1473-3099(13)70690-X.

9. Alagaili AN, Briese T, Mishra N, Kapoor V, Sameroff SC, de Wit E, Munster VJ, Hensley LE, Zalmout IS, Kapoor A, Epstein JH, Karesh WB, Daszak P, Mohammed OB, Lipkin WI. 2014. Middle East respiratory syndrome coronavirus infection in dromedary camels in Saudi Arabia. mBio 5(2):e00884–14. http://dx.doi.org/10.1128/mBio.00884-14.

10. Briese T, Mishra N, Jain K, Zalmout IS, Jabado OJ, Karesh WB, Daszak P, Mohammed OB, Alagaili AN, Lipkin WI. 2014. Middle East respiratory syndrome coronavirus quasispecies that include homologues of human isolates revealed through whole-genome analysis and virus cultured from dromedary camels in Saudi Arabia. mBio 5(3):e01146–14. http://dx.doi.org/10.1128/mBio.01146-14.

11. Cotten M, Watson SJ, Kellam P, Al-Rabeeah AA, Makhdoom HQ, Assiri A, Al-Tawfiq JA, Alhakeem RF, Madani H, Alrabiah FA, Hajjar SA, Al-Nassir WN, Albarrak A, Flemban H, Balkhy HH, Alsubaie S, Palser AL, Gall A, Bashford-Rogers R, Rambaut A, Zumla AI, Memish ZA. 2013. Transmission and evolution of the Middle East respiratory syndrome coronavirus in Saudi Arabia: a descriptive genomic study. Lancet 382:1993–2002. http://dx.doi.org/10.1016/S0140-6736(13)61887-5.

12. Cotten M, Watson SJ, Zumla AI, Makhdoom HQ, Palser AL, Ong SH, Al Rabeeah AA, Alhakeem RF, Assiri A, Al-Tawfiq JA, Albarrak A, Barry M, Shibl A, Alrabiah FA, Hajjar S, Balkhy HH, Flemban H, Rambaut A, Kellam P, Memish ZA. 2014. Spread, circulation, and evolution of the Middle East respiratory syndrome coronavirus. mBio 5(1):e01062–13. http://dx.doi.org/10.1128/mBio.01062-13.

13. Guery B, Poissy J, el Mansouf L, Sejourne C, Ettahar N, Lemaire X, Vuotto F, Goffard A, Behillil S, Enouf V, Caro V, Mailles A, Che D, Manuguerra JC, Mathieu D, Fontanet A, van der Werf S. 2013. Clinical features and viral diagnosis of two cases of infection with Middle East respiratory syndrome coronavirus: a report of nosocomial transmission. Lancet 381:2265–2272. http://dx.doi.org/10.1016/S0140-6736(13)60982-4.

14. Drosten C, Seilmaier M, Corman VM, Hartmann W, Scheible G, Sack S, Guggemos W, Kallies R, Muth D, Junglen S, Muller MA, Haas W, Guberina H, Rohnisch T, Schmid-Wendtner M, Aldabbagh S, Dittmer U, Gold H, Graf P, Bonin F, Rambaut A, Wendtner CM. 2013. Clinical features and virological analysis of a case of Middle East respiratory syndrome coronavirus infection. Lancet Infect. Dis. 13:745–751. http://dx.doi.org/10.1016/S1473-3099(13)70154-3.

15. Li W, Moore MJ, Vasilieva N, Sui J, Wong SK, Berne MA, So-

masundaran M, Sullivan JL, Luzuriaga K, Greenough TC, Choe H, Farzan M. 2003. Angiotensin-converting enzyme 2 is a functional receptor for the SARS coronavirus. Nature 426:450–454. http://dx.doi.org/10.1038/nature02145.

16. Raj VS, Mou H, Smits SL, Dekkers DH, Muller MA, Dijkman R, Muth D, Demmers JA, Zaki A, Fouchier RA, Thiel V, Drosten C, Rottier PJ, Osterhaus AD, Bosch BJ, Haagmans BL. 2013. Dipeptidyl peptidase 4 is a functional receptor for the emerging human coronavirus-EMC. Nature 495:251–254. http://dx.doi.org/10.1038/nature12005.

17. Mou H, Raj VS, van Kuppeveld FJ, Rottier PJ, Haagmans BL, Bosch BJ. 2013. The receptor binding domain of the new Middle East respiratory syndrome coronavirus maps to a 231-residue region in the spike protein that efficiently elicits neutralizing antibodies. J. Virol. 87:9379–9383. http://dx.doi.org/10.1128/JVI.01277-13.

18. Lambeir AM, Durinx C, Scharpe S, De Meester I. 2003. Dipeptidyl-peptidase IV from bench to bedside: an update on structural properties, functions, and clinical aspects of the enzyme DPP IV. Crit. Rev. Clin. Lab. Sci. 40:209–294. http://dx.doi.org/10.1080/713609354.

19. Chan JF, Chan KH, Choi GK, To KK, Tse H, Cai JP, Yeung ML, Cheng VC, Chen H, Che XY, Lau SK, Woo PC, Yuen KY. 2013. Differential cell line susceptibility to the emerging novel human betacoronavirus 2c EMC/2012: implications for disease pathogenesis and clinical manifestation. J. Infect. Dis. 207:1743–1752. http://dx.doi.org/10.1093/infdis/jit123.

20. Kindler E, Jonsdottir HR, Muth D, Hamming OJ, Hartmann R, Rodriguez R, Geffers R, Fouchier RA, Drosten C, Muller MA, Dijkman R, Thiel V. 2013. Efficient replication of the novel human betacoronavirus EMC on primary human epithelium highlights its zoonotic potential. mBio 4(1):e00611–12. http://dx.doi.org/10.1128/mBio.00611-12.

21. Muller MA, Raj VS, Muth D, Meyer B, Kallies S, Smits SL, Wollny R, Bestebroer TM, Specht S, Suliman T, Zimmermann K, Binger T, Eckerle I, Tschapka M, Zaki AM, Osterhaus AD, Fouchier RA, Haagmans BL, Drosten C. 2012. Human coronavirus EMC does not require the SARS-coronavirus receptor and maintains broad replicative capability in mammalian cell lines. mBio 3(6):e00515–12. http://dx.doi.org/10.1128/mBio.00515-12.

22. Chan RW, Chan MC, Agnihothram S, Chan LL, Kuok DI, Fong JH, Guan Y, Poon LL, Baric RS, Nicholls JM, Peiris JS. 2013. Tropism and innate immune responses of the novel human betacoronavirus lineage C virus in human ex vivo respiratory organ cultures. J. Virol. 87:6604–6614. http://dx.doi.org/10.1128/JVI.00009-13.

23. Munster VJ, de Wit E, Feldmann H. 2013. Pneumonia from human coronavirus in a macaque model. N. Engl. J. Med. 368:1560–1562. http://dx.doi.org/10.1056/NEJMc1215691.

24. de Wit E, Prescott J, Baseler L, Bushmaker T, Thomas T, Lackemeyer MG, Martellaro C, Milne-Price S, Haddock E, Haagmans BL, Feldmann H, Munster VJ. 2013. The Middle East respiratory syndrome coronavirus (MERS-CoV) does not replicate in Syrian hamsters. PLoS One 8:e69127. http://dx.doi.org/10.1371/journal.pone.0069127.

25. de Wit E, Rasmussen AL, Falzarano D, Bushmaker T, Feldmann F, Brining DL, Fischer ER, Martellaro C, Okumura A, Chang J, Scott D, Benecke AG, Katze MG, Feldmann H, Munster VJ. 23 September 2013. Middle East respiratory syndrome coronavirus (MERS-CoV) causes transient lower respiratory tract infection in rhesus macaques. Proc. Natl. Acad. Sci. U. S. A. http://dx.doi.org/10.1073/pnas.1310744110.

26. Scobey T, Yount BL, Sims AC, Donaldson EF, Agnihothram SS, Menachery VD, Graham RL, Swanstrom J, Bove PF, Kim JD, Grego S, Randell SH, Baric RS. 16 September 2013. Reverse genetics with a full-length infectious cDNA of the Middle East respiratory syndrome coronavirus. Proc. Natl. Acad. Sci. U. S. A. http://dx.doi.org/10.1073/pnas.1311542110.

27. Enserink M. 2013. New coronavirus reveals some of its secrets. Science 340:17–18. http://dx.doi.org/10.1126/science.340.6128.17.

28. Raj VS, Smits SL, Provacia LB, van den Brand JM, Wiersma L, Ouwendijk WJ, Bestebroer TM, Spronken MI, van Amerongen G, Rottier PJ, Fouchier RA, Bosch BJ, Osterhaus AD, Haagmans BL. 2014. Adenosine deaminase acts as a natural antagonist for dipeptidyl peptidase 4-mediated entry of the Middle East respiratory syndrome coronavirus. J. Virol. 88:1834–1838. http://dx.doi.org/10.1128/JVI.02935-13.

29. Cockrell AS, Peck KM, Yount BL, Agnihothram SS, Scobey T, Curnes NR, Baric RS, Heise MT. 26 February 2014. Mouse dipeptidyl peptidase 4 (DPP4) is not a functional receptor for Middle East respiratory syndrome coronavirus (MERS-CoV) infection. J. Virol. http://dx.doi.org/10.1128/JVI.03764-13.

30. **Barlan A, Zhao J, Sarkar MK, Li K, McCray PB, Jr, Perlman S, Gallagher T.** 19 February 2014. Receptor variation and susceptibility to MERS coronavirus infection. J. Virol. http://dx.doi.org/10.1128/JVI.00161-14.

31. **Larkin MA, Blackshields G, Brown NP, Chenna R, McGettigan PA, McWilliam H, Valentin F, Wallace IM, Wilm A, Lopez R, Thompson JD, Gibson TJ, Higgins DG.** 2007. Clustal W and Clustal X version 2.0. Bioinformatics **23:**2947–2948. http://dx.doi.org/10.1093/bioinformatics/btm404.

32. **Petrey D, Xiang Z, Tang CL, Xie L, Gimpelev M, Mitros T, Soto CS, Goldsmith-Fischman S, Kernytsky A, Schlessinger A, Koh IY, Alexov E, Honig B.** 2003. Using multiple structure alignments, fast model building, and energetic analysis in fold recognition and homology modeling. Proteins **53**(Suppl 6)**:**S430–S435. http://dx.doi.org/10.1002/prot.10550.

33. **Ponder JW.** 1999. TINKER—software tools for molecular design, version 3.7. Washington University, St. Louis, MO.

34. **Zhou H, Zhou Y.** 2002. Distance-scaled, finite ideal-gas reference state improves structure-derived potentials of mean force for structure selection and stability prediction. Protein Sci. **11:**2714–2726. http://dx.doi.org/10.1110/ps.0217002.

35. **Livak KJ, Schmittgen TD.** 2001. Analysis of relative gene expression data using real-time quantitative PCR and the 2(-delta delta C(T)) method. Methods **25:**402–408. http://dx.doi.org/10.1006/meth.2001.1262.

36. **Lu G, Hu Y, Wang Q, Qi J, Gao F, Li Y, Zhang Y, Zhang W, Yuan Y, Bao J, Zhang B, Shi Y, Yan J, Gao GF.** 2013. Molecular basis of binding between novel human coronavirus MERS-CoV and its receptor CD26. Nature **500:**227–231. http://dx.doi.org/10.1038/nature12328.

37. **Wang N, Shi X, Jiang L, Zhang S, Wang D, Tong P, Guo D, Fu L, Cui Y, Liu X, Arledge KC, Chen YH, Zhang L, Wang X.** 2013. Structure of MERS-CoV spike receptor-binding domain complexed with human receptor DPP4. Cell Res. **23:**986–993. http://dx.doi.org/10.1038/cr.2013.92.

38. **McIntosh K.** 2013. A new virulent human coronavirus: how much does tissue culture tropism tell us? J. Infect. Dis. **207:**1630–1632. http://dx.doi.org/10.1093/infdis/jit125.

39. **Falzarano D, de Wit E, Rasmussen AL, Feldmann F, Okumura A, Scott DP, Brining D, Bushmaker T, Martellaro C, Baseler L, Benecke AG, Katze MG, Munster VJ, Feldmann H.** 2013. Treatment with interferon-alpha2b and ribavirin improves outcome in MERS-CoV-infected rhesus macaques. Nat. Med. **19:**1313–1317. http://dx.doi.org/10.1038/nm.3362.

40. **Falzarano D, de Wit E, Martellaro C, Callison J, Munster VJ, Feldmann H.** 2013. Inhibition of novel beta coronavirus replication by a combination of interferon-alpha2b and ribavirin. Sci. Rep. **3:**1686. http://dx.doi.org/10.1038/srep01686.

41. **Song F, Fux R, Provacia LB, Volz A, Eickmann M, Becker S, Osterhaus AD, Haagmans BL, Sutter G.** 2013. Middle East respiratory syndrome coronavirus spike protein delivered by modified vaccinia virus Ankara efficiently induces virus-neutralizing antibodies. J. Virol. **87:**11950–11954. http://dx.doi.org/10.1128/JVI.01672-13.

42. **Almazan F, DeDiego ML, Sola I, Zuniga S, Nieto-Torres JL, Marquez-Jurado S, Andres G, Enjuanes L.** 2013. Engineering a replication-competent, propagation-defective Middle East respiratory syndrome coronavirus as a vaccine candidate. mBio. **4**(5)**:**e00650–13. http://dx.doi.org/10.1128/mBio.00650-13.

43. **Zhao J, Li K, Wohlford-Lenane C, Agnihothram SS, Fett C, Gale MJ, Jr, Baric RS, Enjuanes L, Gallagher T, McCray PB, Jr, Perlman S.** 5 March 2014. Rapid generation of a mouse model for Middle East respiratory syndrome. Proc. Natl. Acad. Sci. U. S. A. http://dx.doi.org/10.1073/pnas.1323279111.

44. **Reusken CB, Ababneh M, Raj VS, Meyer B, Eljarah A, Abutarbush S, Godeke GJ, Bestebroer TM, Zutt I, Muller MA, Bosch BJ, Rottier PJ, Osterhaus AD, Drosten C, Haagmans BL, Koopmans MP.** 2013. Middle East respiratory syndrome coronavirus (MERS-CoV) serology in major livestock species in an affected region in Jordan, June to September 2013. Euro Surveill. **18:**pii=20662. http://www.eurosurveillance.org/ViewArticle.aspx?ArticleId=20662.